
Article:
Chen, L., Li, B. and de Borst, R. orcid.org/0000-0002-3457-3574 (2024) Integral form of mixed-mode crack opening in the phase field method. Theoretical and Applied Fracture Mechanics, 132. 104481. ISSN 0167-8442

https://doi.org/10.1016/j.tafmec.2024.104481

Theoretical and Applied Fracture Mechanics 132 (2024) 104481

Contents lists available at ScienceDirect

Theoretical and Applied Fracture Mechanics

journal homepage: www.elsevier.com/locate/tafmec

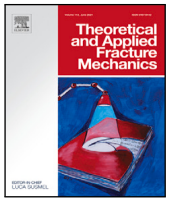

Integral form of mixed-mode crack opening in the phase field method

Lin Chen [a], Bin Li [b], René de Borst [c,*]

[a] Northeastern University, Key Laboratory of Ministry of Education on Safe Mining of Deep Metal Mines, Shenyang 110819, China
[b] Guangdong Technion-Israel Institute of Technology, Department of Mechanical Engineering, Shantou 515063, China
[c] University of Sheffield, Department of Civil and Structural Engineering, Sheffield S1 3JD, UK

ARTICLE INFO

Keywords:
Crack opening
Phase field model
Smeared crack
Brittle fracture
Cohesive fracture

ABSTRACT

Phase-field modelling of cracks has gained popularity in the fracturing analysis recently. Originally developed for brittle fracture, the method has now been extended to cohesive fracture. In the latter case, the crack opening displacement is an essential variable, due to the dependence on it of the interface tractions. But also in brittle fracture, the crack opening displacement is crucial in certain applications, for instance for transport of fluids in the cracks. Herein, we derive the complete formulation for mixed-mode crack opening within the framework of the phase-field model, given for brittle as well as for cohesive fracture. The crack opening displacement is associated with a line integral that is perpendicular to the crack. Different factors and matrices apply in the integration for both fracture models and crack directions. These derivations have been validated analytically through an edge-cracked problem and numerically through curved crack scenarios.

1. Introduction

The phase-field model has been employed widely in the analysis of fracturing. The first contribution is by Bourdin, Francfort and Marigo, e.g., [1]. The crack is regularised in a smeared sense, and described by a scalar phase-field variable d [2]. The width of the smeared crack is set by an internal length scale ℓ. There is no need to introduce geometric discontinuities in describing the cracks, and remeshing around the crack tips is not necessary, although it can be useful to increase the accuracy or to reduce the computational costs.

The vast majority of the phase-field models have been applied in the analysis of brittle fracture [3], encompassing ductile fractures [4], fatigue analysis [5], hydraulic fracturing [6], and dynamic fracture [7], among others. In the brittle fracture model, the crack initiation and quasi-static propagation is governed by a minimisation problem of an energy functional [8].

Different from fracture that is induced by an external load, hydraulic fracturing is a physical process caused by the fluid pressure in the crack [9]. For the fluid flow in the crack, the Reynolds flow model, which relies on the crack opening displacement, is typically employed [4]. Several approaches have been proposed for the computation of the normal crack opening [3,6]. Often, a line integral is used for its computation [9]. However, the computation of the crack opening in the shear direction is underdeveloped. The shear crack opening is crucial in considering the shear traction along the crack surface, such as the fluid shear stress [10].

Phase-field models have also been cast in the framework of cohesive fracture [11]. The first extension of the phase-field approach to the cohesive fracture was by Verhoosel and de Borst [11]. The interface tractions depend on the crack opening. Verhoosel and de Borst [11] treated the cohesive interface in a smeared sense by the phase-field regularisation technique, and introduced an auxiliary field to model the crack opening, see also [12–15]. Nguyen et al. [16] adopted a similar regularisation strategy to represent the cohesive interface. They avoided the auxiliary field by computing the displacement jump at two points near the interface. However, the choice of the location of these points seems arbitrary and problem-dependent. Recently, de Borst and Chen [17] derived the analytical form of the crack opening and obtained the optimal location of these points. Lee et al. [18] and Yoshioka et al. [9] used a level-set approach to obtain the crack normal vector, and this is applied in the computation of the displacement jump. The accuracy of this approach depends on the level set function.

Obviously, the displacements at the crack, including the normal and shear components, are crucial variables in the cohesive fracture model and also in certain applications of the brittle fracture model, e.g., in hydraulic fracturing. This study will focus on the general case of the computation of the displacements at the crack within the framework of phase-field modelling. The formulations will be given for the normal and shear components of the displacement jump at the crack. The line integral form of the displacements at the crack will be derived for the brittle as well as for the cohesive fracture model. Validation of

* Corresponding author.
E-mail address: r.deborst@sheffield.ac.uk (R. de Borst).

https://doi.org/10.1016/j.tafmec.2024.104481
Received 22 February 2024; Received in revised form 17 April 2024; Accepted 22 May 2024
Available online 27 May 2024

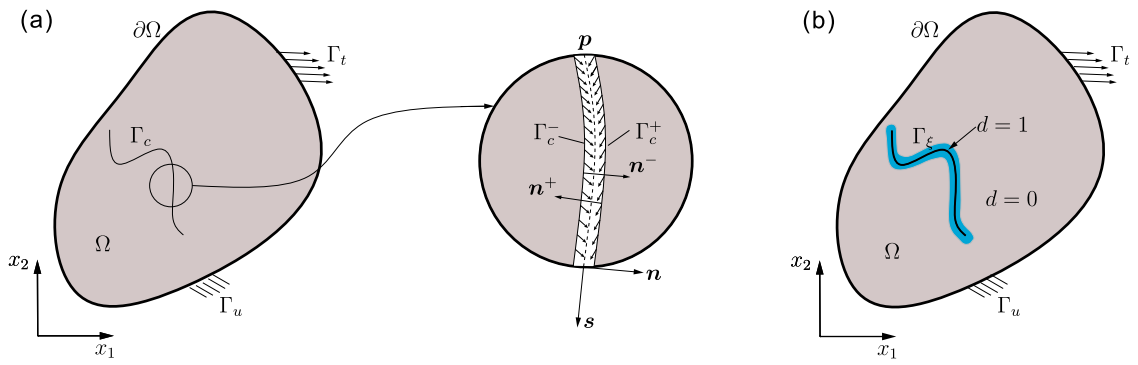

Fig. 1. (a) a solid body $\boldsymbol{\Omega}$ with a discrete crack Γ_c. Γ_c is the crack boundary with positive and negative sides, Γ_c^+ and Γ_c^-, respectively. Boundary Γ_u is prescribed with a displacement $\bar{\mathbf{u}}$; Γ_t with a prescribed traction $\hat{\mathbf{t}}$; (b) a solid body $\boldsymbol{\Omega}$ with a smeared interface Γ_ξ (blue area).

the proposed formula is provided by an edge-cracked problem where analytical solutions are available. We will start this contribution with a concise description of phase-field modelling of fractures. Subsequently, the displacements at the crack are derived for the normal and for the shear components, respectively. The theoretical validation is given in Section 4. Finally, we will consider two examples with complex crack patterns to numerically validate the approach and conclusions are drawn.

2. Phase field model for fracture

We now briefly summarise phase-field modelling of brittle and cohesive fracture. Fig. 1 presents an open domain Ω with an internal discontinuity Γ_c. Γ_c can either be a brittle fracture or a cohesive crack. Tractions $\boldsymbol{p}$ on Γ_c can either refer to tractions on the brittle fracture surface, or cohesive tractions. Infinitesimal strains, linear elastic material behaviour and the absence of body force have been assumed.

2.1. Smeared crack representation

In the phase-field modelling, the crack geometry is not traced explicitly [1]. Instead, it is approximated by a smeared representation Γ_ξ, as shown in Fig. 1(b). Γ_ξ is associated with an evolving phase field $d(\mathbf{x})$, which satisfies following conditions: $d(\mathbf{x}) = 1$ at the centre of the crack Γ_c, and $d(\mathbf{x})$ vanishing gradually away from Γ_c. The width of the smeared crack Γ_ξ is described by a regularisation parameter ℓ. The distribution of $d(\mathbf{x})$ is determined by solving a variational problem:

$$d(\mathbf{x}) = \text{Arg}\left\{\inf_{d\in S_d} \quad \Gamma_d(d)\right\} \qquad \text{with} \qquad \Gamma_d(d) = \int_\Omega \gamma_d(d)\,\mathrm{d}V \quad (1)$$

where $S_d = \left\{ d \,\middle|\, d(\mathbf{x}) = 1 \;\forall \mathbf{x} \in \Gamma_c \right\}$. Γ_d represents the total crack length per unit area. $\gamma_d(d)$ is the crack density function per unit volume. It has the unit of the inverse of a length and is given as:

$$\gamma_d(d) = \frac{1}{\pi\ell}\left(2d(\mathbf{x}) - d(\mathbf{x})^2\right) + \frac{\ell}{\pi}\nabla d(\mathbf{x})\cdot\nabla d(\mathbf{x}) \quad (2)$$

For $\ell \to 0$, the variational form in Eq. (1) leads to the exact description of the sharp crack topology Γ_c. The Euler–Lagrange equation associated with the variational Eq. (1) reads:

$$\begin{aligned} 1 - d(x_n) - \ell^2 \frac{\mathrm{d}^2 d(x_n)}{\mathrm{d}x_n^2} = 0 \qquad & x_n \in \mathbb{R} \\ d = 1 \qquad & x_n = 0 \\ d = 0 \qquad & x_n = (-\infty, -\pi\ell/2] \bigcup [\pi\ell/2, +\infty) \end{aligned} \quad (3)$$

with $x_n = (\mathbf{x} - \mathbf{x}_c)\cdot\boldsymbol{n}(\mathbf{x}_c)$, point $\mathbf{x}_c$ on the crack Γ_c and $\boldsymbol{n}(\mathbf{x}_c)$ the unit vector normal to Γ_c. The solution of the Euler–Lagrange equation is given by:

$$d(x_n) = \begin{cases} 1 - \sin\left(\dfrac{|x_n|}{\ell}\right) & -\pi\ell/2 \le x_n \le \pi\ell/2 \\ 0 & \text{otherwise} \end{cases} \quad (4)$$

Chen et al. [19] have presented the plot of the phase-field $d(x_n)$ and the crack density function $\gamma_d(d)$. In their analysis, the distribution of $d(x_n)$ and $\gamma_d(d)$ is localised around the crack Γ_c, confining the influence of the smeared crack Γ_ξ. This is a superior aspect of the current phase-field model over the classical phase field model (also known as AT2) [19].

2.2. Regularised brittle fracture model

We consider a cracked body $\Omega \subseteq \mathcal{R}^n$, with prescribed tractions $\boldsymbol{p}$ on Γ_c. $\boldsymbol{p} = [p_f, t_f]$ includes the pressure p_f exerted on the crack surface, such as the fluid pressure in the hydraulic fracturing [6,9], and the shear traction t_f along the crack surface, including the fluid shear stress [10]. The potential $\mathcal{P}(\mathbf{u}, \Gamma; \boldsymbol{p})$ for the cracked body is then written as

$$\begin{aligned} \mathcal{P}(\mathbf{u}, \Gamma; \boldsymbol{p}) = & \int_{\Omega\setminus\Gamma} \mathcal{W}(\mathbf{u})\,\mathrm{d}\Omega - \int_{\Gamma_t} \mathbf{u}\cdot\hat{\mathbf{t}}\,\mathrm{d}\Gamma - \int_{\Gamma_c} p_f \llbracket \mathbf{u}\cdot\boldsymbol{n}\rrbracket\,\mathrm{d}\Gamma \\ & - \int_{\Gamma_c} t_f \llbracket \mathbf{u}\cdot\boldsymbol{s}\rrbracket\,\mathrm{d}\Gamma \end{aligned} \quad (5)$$

where $\hat{\mathbf{t}}$ is the prescribed traction on the boundary Γ_t, $\mathcal{W}(\mathbf{u})$, $\mathcal{W}(\mathbf{u}) = \mu\boldsymbol{\varepsilon}(\mathbf{u})\cdot\boldsymbol{\varepsilon}(\mathbf{u}) + \lambda/2\text{tr}(\boldsymbol{\varepsilon}(\mathbf{u}))^2$ is the energy density function, with λ and μ the Lamé constants, and $\boldsymbol{\varepsilon}(\mathbf{u}) = 1/2\left(\nabla\mathbf{u} + \nabla\mathbf{u}^{\mathrm{T}}\right)$ is the strain. $\llbracket \mathbf{u}\cdot\boldsymbol{n}\rrbracket$ and $\llbracket \mathbf{u}\cdot\boldsymbol{s}\rrbracket$ are the displacements at the crack in the normal and shear directions, respectively.

Minimising Eq. (5) is a challenging task, considering phenomena like crack initiation, unstable propagation, tortuous crack paths, branching, multiple crack interaction, coalescence and merging. Phase-field modelling of crack propagation introduces a variational discontinuity-free formulation of brittle fracture, and considers the crack geometry and the displacement field simultaneously [2]. The crack initiation and evolution are governed by a minimisation of a Griffith-like energy functional. The method relies on a regularised description of the discontinuity [1]. In the regularised model, cracks are represented by a scalar phase field, or damage variable, d, which attains the value 1 in a completely broken state and 0 away from the crack, and varies smoothly between 0 to 1 over a finite width. Then, the energy functional, Eq. (5), is replaced by [1]:

$$\begin{aligned} \mathcal{E}(\mathbf{u}, \Gamma; \boldsymbol{p}) = & \int_\Omega a(d)\,\mathcal{W}(\mathbf{u})\,\mathrm{d}\Omega - \int_{\Gamma_t} \mathbf{u}\cdot\hat{\mathbf{t}}\,\mathrm{d}\,\Gamma - \int_{\Gamma_c} p_f \llbracket \mathbf{u}\cdot\boldsymbol{n}\rrbracket\,\mathrm{d}\Gamma \\ & - \int_{\Gamma_c} t_f \llbracket \mathbf{u}\cdot\boldsymbol{s}\rrbracket\,\mathrm{d}\Gamma + \mathcal{G}_c \int_\Omega \gamma_d(d)\,\mathrm{d}\Omega \end{aligned} \quad (6)$$

in which $a(d) = (1-d)^2$ denotes a degradation function, $\gamma_d(d)$ is the crack density function per unit volume, defined in Eq. (2). The last term represents the fracture surface energy in the sense of Griffith's theory of brittle fracture [2]. Inh Eq. (6) $\int_{\Gamma_c} p_f \llbracket \mathbf{u}\cdot\boldsymbol{n}\rrbracket\,\mathrm{d}\Gamma$ and $\int_{\Gamma_c} t_f \llbracket \mathbf{u}\cdot\boldsymbol{s}\rrbracket\,\mathrm{d}\Gamma$ are still in a discrete format, i.e. not regularised, due to unknown locations of the crack opening [6]. The regularised forms of $\int_{\Gamma_c} p_f \llbracket \mathbf{u}\cdot\boldsymbol{n}\rrbracket\,\mathrm{d}\Gamma$ and $\int_{\Gamma_c} t_f \llbracket \mathbf{u}\cdot\boldsymbol{s}\rrbracket\,\mathrm{d}\Gamma$ will be given in Section 3.

2.3. Regularised cohesive fracture model

The cohesive-zone model [20,21] is widely employed to model fracture, especially in quasi-brittle and ductile materials. It essentially relates the tractions on a crack surface Γ_c to the displacement jumps at the crack, as shown in Fig. 1(a). The cohesive-zone relation is defined as:

$$\boldsymbol{p} = \mathbf{t}_d\left(\llbracket \boldsymbol{v} \rrbracket, \boldsymbol{\kappa}\right) \tag{7}$$

where $\boldsymbol{\kappa}$ is a history parameter, obeying Kuhn–Tucker conditions to distinguish between loading and unloading. $\boldsymbol{p}$ are the cohesive tractions $\mathbf{t}_d$ acting on Γ_c. $\llbracket \boldsymbol{v} \rrbracket$ denotes the displacement jump over the crack, with components in the normal and shear directions. $\mathbf{t}_d$ and $\llbracket \boldsymbol{v} \rrbracket$ are given in the local coordinate system (s, n), see Fig. 1. The traction $\mathbf{t}$ and the crack opening $\llbracket \mathbf{u} \rrbracket$ in the global coordinate system (x_1, x_2) are obtained via a standard transformation:

$$\mathbf{t} = \mathbf{R}^{\mathrm{T}}\mathbf{t}_d, \qquad \llbracket \mathbf{u} \rrbracket = \mathbf{u}^{+} - \mathbf{u}^{-} = \mathbf{R}^{\mathrm{T}}\left[\llbracket \mathbf{u}\cdot s \rrbracket \;\; \llbracket \mathbf{u}\cdot n \rrbracket\right]^{\mathrm{T}} \tag{8}$$

with $\mathbf{R}$ being a rotation matrix [22,23]. $\mathbf{u}^{+}$ and $\mathbf{u}^{-}$ are the displacements on the positive and negative sides, Γ_c^{+} and Γ_c^{-} of the crack, respectively, see Fig. 1.

The original works on cohesive-zone models treat the crack interface Γ_c as a geometric discontinuity. The cohesive tractions $\boldsymbol{p}$ are applied directly on the discrete interface [22] and the energy functional reads:

$$\mathcal{E}\left(\mathbf{u}, \Gamma; \boldsymbol{p}\right) = \int_{\Omega} \mathcal{W}(\mathbf{u})\,\mathrm{d}\Omega - \int_{\Gamma_t} \mathbf{u}\cdot\hat{\mathbf{t}}\,\mathrm{d}\Gamma + \int_{\Gamma} \mathcal{G}\left(\llbracket \mathbf{u} \rrbracket, \boldsymbol{\kappa}\right)\mathrm{d}A \tag{9}$$

where $\mathcal{G}\left(\llbracket \mathbf{u} \rrbracket, \boldsymbol{\kappa}\right)$ is the fracture energy function, representing the energy dissipation upon the creation of a unit crack surface. It is released gradually in cohesive zone models, linking to the cohesive tractions by a differential form:

$$\boldsymbol{p} = \frac{\partial \mathcal{G}\left(\llbracket \mathbf{u} \rrbracket, \boldsymbol{\kappa}\right)}{\partial \llbracket \mathbf{u} \rrbracket} \tag{10}$$

More recently, cohesive-zone models have been cast in the phase-field format [11,14]. The cohesive fracture Γ_c is regularised by the phase field [15], resulting in a smeared crack, Γ_ξ in Fig. 1(b). The infinitesimal area $\mathrm{d}A$ in Eq. (9), at every point $\boldsymbol{x}_c$ on the interface Γ_c, can be expressed in an integral form:

$$\mathrm{d}A\left(\boldsymbol{x}_c\right) = \underbrace{\int_{x_n=-\infty}^{\infty} \delta\left(x_n\right)\mathrm{d}x_n}_{=1}\mathrm{d}A = \int_{x_n=-\infty}^{\infty} \delta\left(x_n\right)\mathrm{d}V \approx \int_{x_n=-\infty}^{\infty} \delta_c\left(x_n\right)\mathrm{d}V \tag{11}$$

with $x_n = \left(\mathbf{x} - \mathbf{x}_c\right)\cdot\boldsymbol{n}\left(\mathbf{x}_c\right)$ and $\boldsymbol{n}\left(\mathbf{x}_c\right)$ the unit vector normal to the crack Γ_c. In a simulation, we cannot directly use $\delta\left(x_n\right)$ due to the jump in $\delta\left(x_n\right)$. Thus, we consider an approximation, $\delta_c\left(x_n\right)$, in the integrated format. A possibility is to use the crack density function $\gamma_d\left(d\right)$ to replace $\delta_c\left(x_n\right)$ [15]. In current study, in order to simplify the computation, we use following approximation:

$$\begin{aligned}\delta_c\left(x_n\right) = \frac{1}{2}\left|\frac{\mathrm{d}d\left(x_n\right)}{\mathrm{d}x_n}\right| &= \frac{1}{2}\begin{cases} -\dfrac{\mathrm{d}d\left(x_n\right)}{\mathrm{d}x_n} & 0 < x_n \le \pi\ell/2 \\ \dfrac{\mathrm{d}d\left(x_n\right)}{\mathrm{d}x_n} & -\pi\ell/2 \le x_n \le 0 \\ 0 & \text{otherwise}\end{cases} \\ &= \frac{1}{2}\begin{cases} \dfrac{1}{\ell}\cos\left(\dfrac{x_n}{\ell}\right) & -\pi\ell/2 \le x_n \le \pi\ell/2 \\ 0 & \text{otherwise}\end{cases}\end{aligned} \tag{12}$$

in which the fraction $\frac{1}{2}$ stems from the constraint on the Dirac-delta function, $\int_{-\infty}^{\infty}\delta_c\left(x_n\right)\mathrm{d}x_n = 1$. The function $\delta_c\left(x_n\right)$ is localised around the crack Γ_c.

Substitution of Eq. (11) into the energy functional, Eq. (9), yields a phase-field regularised energy function for cohesive fracture [15]:

$$\begin{aligned}\mathcal{E}\left(\mathbf{u}, \Gamma; \boldsymbol{p}\right) &= \int_{\Omega} \mathcal{W}(\mathbf{u})\,\mathrm{d}\Omega - \int_{\Gamma_t} \mathbf{u}\cdot\hat{\mathbf{t}}\,\mathrm{d}\Gamma + \int_{\Gamma} \mathcal{G}\left(\llbracket \mathbf{u} \rrbracket, \boldsymbol{\kappa}\right)\int_{x_n=-\infty}^{\infty}\delta\left(x_n\right)\mathrm{d}V \\ &\approx \int_{\Omega} \mathcal{W}(\mathbf{u})\,\mathrm{d}\Omega - \int_{\Gamma_t} \mathbf{u}\cdot\hat{\mathbf{t}}\,\mathrm{d}\Gamma + \int_{\Omega} \mathcal{G}\left(\llbracket \mathbf{u} \rrbracket, \boldsymbol{\kappa}\right)\delta_c\left(x_n\right)\mathrm{d}V\end{aligned} \tag{13}$$

Due to the localisation property of $\delta_c\left(x_n\right)$ the integral $\int_{x_n=-\infty}^{\infty}\delta_c\left(x_n\right)\mathrm{d}V$ is confined in a localised area, different from the classical phase field model (also known as AT2), in simulations of Verhoosel and de Borst [11].

3. Mixed-mode crack opening/sliding in the phase-field method

Due to the untracked crack geometry in the variational approach to fracture, the crack opening in Eqs. (6) and (13) cannot be computed directly in the phase-field model. Chukwudozie et al. [6] proposed an integral form to compute the crack opening in the normal direction for the analysis of hydraulic fracturing in brittle porous media. The extension to the crack opening computation in the shear direction and to cohesive fracture model is still open. In this section, we elaborate on the crack opening computation for brittle and cohesive fracture.

3.1. Crack opening/sliding for brittle fracture

The basic concept of the phase-field model is to regularise the crack Γ_c by a smeared representation Γ_ξ, as presented in Fig. 1(b). In the regularised phase-field model, the discrete form $\int_{\Gamma_c} p_f\,\llbracket \mathbf{u}\cdot\boldsymbol{n} \rrbracket\,\mathrm{d}\Gamma$ can be reformulated in the following smeared approximation [6]:

$$\int_{\Gamma_c} p_f\,\llbracket \mathbf{u}\cdot\boldsymbol{n} \rrbracket\,\mathrm{d}\Gamma \approx -\int_{\Omega} p_f\mathbf{u}\cdot\nabla d\,\mathrm{d}\Omega \tag{14}$$

where the minus sign in front of the integration stems from the definition of the phase field variable d, being different from that of Chukwudozie et al. [6].

Integrating the phase-field gradient in the normal direction $\boldsymbol{n}$ leads to

$$\int_{-\infty}^{0}\left|\nabla d\left(x_n\right)\right|\mathrm{d}x_n = \int_{0}^{\infty}\left|\nabla d\left(x_n\right)\right|\mathrm{d}x_n = 1 \tag{15}$$

where $x_n = \left(\mathbf{x} - \mathbf{x}_c\right)\cdot\boldsymbol{n}\left(\mathbf{x}_c\right)$, point $\mathbf{x}_c$ on the crack Γ_c and $\boldsymbol{n}\left(\mathbf{x}_c\right)$ the unit vector normal to the crack Γ_c. The crack opening $\llbracket \mathbf{u} \rrbracket$ then reads:

$$\begin{aligned}\llbracket \mathbf{u} \rrbracket = \mathbf{u}\left(x_n^{+}\right) - \mathbf{u}\left(x_n^{-}\right) &= \mathbf{u}\left(x_n^{+}\right)\int_{0}^{\infty}\left|\nabla d\left(x_n\right)\right|\mathrm{d}x_n \\ &- \mathbf{u}\left(x_n^{-}\right)\int_{-\infty}^{0}\left|\nabla d\left(x_n\right)\right|\mathrm{d}x_n\end{aligned} \tag{16}$$

x_n^{+} and x_n^{-} being points on positive and negative sides of the crack Γ_c.

Due to the localised support of the current phase-field model [19], we can consider $\mathbf{u}\left(x_n^{+}\right)$ and $\mathbf{u}\left(x_n^{-}\right)$ as constants in the direction normal to the crack. The crack opening in the normal direction has following form:

$$\begin{aligned}\llbracket \mathbf{u}\cdot\boldsymbol{n} \rrbracket = \mathbf{u}\left(x_n^{+}\right)\cdot\boldsymbol{n} - \mathbf{u}\left(x_n^{-}\right)\cdot\boldsymbol{n} &= \mathbf{u}\left(x_n^{+}\right)\cdot\boldsymbol{n}\int_{0}^{\infty}\left|\nabla d\left(x_n\right)\right|\mathrm{d}x_n \\ &- \mathbf{u}\left(x_n^{-}\right)\cdot\boldsymbol{n}\int_{-\infty}^{0}\left|\nabla d\left(x_n\right)\right|\mathrm{d}x_n \\ &\approx \int_{0}^{\infty}\mathbf{u}\left(x_n\right)\cdot\boldsymbol{n}\left|\nabla d\left(x_n\right)\right|\mathrm{d}x_n \\ &- \int_{-\infty}^{0}\mathbf{u}\left(x_n\right)\cdot\boldsymbol{n}\left|\nabla d\left(x_n\right)\right|\mathrm{d}x_n\end{aligned} \tag{17}$$

The normal vector $\boldsymbol{n}$ can be approximated as [6]

$$\boldsymbol{n} \approx -\nabla d\left(x_n^{+}\right)\mathbf{I}\Big/\left|\nabla d\left(x_n^{+}\right)\right| = -\frac{1}{\left|\nabla d\left(x_n^{+}\right)\right|}\left[\frac{\partial d\left(x_n^{+}\right)}{\partial x_1} \;\; \frac{\partial d\left(x_n^{+}\right)}{\partial x_2}\right]$$

$$\approx \nabla d\left(x_n^-\right)\mathbf{I} \Big/ \left|\nabla d\left(x_n^-\right)\right| \tag{18}$$

with $\left|\nabla d\left(x_n^+\right)\right| = \sqrt{\left(\frac{\partial d(x_n^+)}{\partial x_1}\right)^2 + \left(\frac{\partial d(x_n^+)}{\partial x_2}\right)^2}$, and $\mathbf{I}$ a 2×2 identity matrix. Substituting Eq. (18) into Eq. (17) yields the approximated form of the crack opening in the normal direction:

$$[\![\mathbf{u}\cdot\boldsymbol{n}]\!] \approx -\int_{-\infty}^{\infty} \mathbf{u}\left(x_n\right)\cdot\left(\nabla d\left(x_n\right)\mathbf{I}\right)\mathrm{d}x_n \approx -\int_{-\pi\ell/2}^{\pi\ell/2} \mathbf{u}\left(x_n\right)\cdot\left(\nabla d\left(x_n\right)\mathbf{I}\right)\mathrm{d}x_n \tag{19}$$

where Eq. (4) has been used.

The unit shear vector $\boldsymbol{s}$ along the crack Γ_c, see Fig. 1(a), can be obtained from

$$\begin{aligned}\boldsymbol{s}_{3d} = \boldsymbol{n}_{3d}\times\boldsymbol{z} &\approx \frac{1}{\left|\nabla d\left(x_n^+\right)\right|}\left[-\frac{\partial d\left(x_n^+\right)}{\partial x_2} \quad \frac{\partial d\left(x_n^+\right)}{\partial x_1} \quad 0\right]\\ &\approx \frac{1}{\left|\nabla d\left(x_n^-\right)\right|}\left[\frac{\partial d\left(x_n^-\right)}{\partial x_2} \quad -\frac{\partial d\left(x_n^-\right)}{\partial x_1} \quad 0\right]\end{aligned} \tag{20}$$

where $\boldsymbol{n}_{3d} = [\boldsymbol{n}\ 0]$, $\boldsymbol{z} = [0\ 0\ 1]$, and $\boldsymbol{s}_{3d}$ is given in the three-dimensional space. In two-dimensional simulations we only need to consider the first two terms:

$$\begin{aligned}\boldsymbol{s} &\approx \frac{1}{\left|\nabla d\left(x_n^+\right)\right|}\left[-\frac{\partial d\left(x_n^+\right)}{\partial x_2} \quad \frac{\partial d\left(x_n^+\right)}{\partial x_1}\right] = \frac{-\nabla d\left(x_n^+\right)\mathbf{I}_a}{\left|\nabla d\left(x_n^+\right)\right|}\\ &\approx \frac{1}{\left|\nabla d\left(x_n^-\right)\right|}\left[\frac{\partial d\left(x_n^-\right)}{\partial x_2} \quad -\frac{\partial d\left(x_n^-\right)}{\partial x_1}\right] = \frac{\nabla d\left(x_n^-\right)\mathbf{I}_a}{\left|\nabla d\left(x_n^-\right)\right|}\end{aligned} \tag{21}$$

with $\mathbf{I}_a = \begin{bmatrix}1 & 0\\ 0 & -1\end{bmatrix}$. Then, the crack sliding in the shear direction can be approximated as:

$$\begin{aligned}[\![\mathbf{u}\cdot\boldsymbol{s}]\!] = \mathbf{u}\left(x_n^+\right)\cdot\boldsymbol{s} - \mathbf{u}\left(x_n^-\right)\cdot\boldsymbol{s} &= \mathbf{u}\left(x_n^+\right)\cdot\boldsymbol{s}\int_0^{\infty}\left|\nabla d\left(x_n\right)\right|\mathrm{d}x_n\\ &\quad - \mathbf{u}\left(x_n^-\right)\cdot\boldsymbol{s}\int_{-\infty}^{0}\left|\nabla d\left(x_n\right)\right|\mathrm{d}x_n\\ &\approx \int_0^{\infty}\mathbf{u}\left(x_n\right)\cdot\boldsymbol{s}\left|\nabla d\left(x_n\right)\right|\mathrm{d}x_n\\ &\quad - \int_{-\infty}^{0}\mathbf{u}\left(x_n\right)\cdot\boldsymbol{s}\left|\nabla d\left(x_n\right)\right|\mathrm{d}x_n\\ &\approx -\int_{-\infty}^{\infty}\mathbf{u}\left(x_n\right)\\ &\quad\cdot\left[\frac{\partial d\left(x_n\right)}{\partial x_2} \quad -\frac{\partial d\left(x_n\right)}{\partial x_1}\right]\mathrm{d}x_n\\ &= -\int_{-\pi\ell/2}^{\pi\ell/2}\mathbf{u}\left(x_n\right)\cdot\left(\nabla d\left(x_n\right)\mathbf{I}_a\right)\mathrm{d}x_n\end{aligned} \tag{22}$$

and the discrete term $\int_{\Gamma_c} t_f\,[\![\mathbf{u}\cdot\boldsymbol{s}]\!]\,\mathrm{d}\Gamma$ in Eq. (6) is given as

$$\int_{\Gamma_c} t_f\,[\![\mathbf{u}\cdot\boldsymbol{s}]\!]\,\mathrm{d}\Gamma \approx -\int_{\Omega} t_f\mathbf{u}\cdot\left(\nabla d\mathbf{I}_a\right)\mathrm{d}\Omega \tag{23}$$

Hence, the crack sliding for brittle fracture can be approximated as:

$$\left[[\![\mathbf{u}\cdot\boldsymbol{n}]\!] \quad [\![\mathbf{u}\cdot\boldsymbol{s}]\!]\right] \approx -\int_{-\infty}^{\infty}\left[\mathbf{u}\left(x_n\right)\cdot\left(\nabla d\left(x_n\right)\mathbf{I}\right) \quad \mathbf{u}\left(x_n\right)\cdot\left(\nabla d\left(x_n\right)\mathbf{I}_a\right)\right]\mathrm{d}x_n \tag{24}$$

3.2. Crack opening/sliding for cohesive fracture

In the cohesive fracture model the crack opening $[\![\mathbf{u}]\!]$ can be regularised by using the Dirac-delta function:

$$\begin{aligned}[\![\mathbf{u}]\!]\left(\boldsymbol{x}_c\right) &= \underbrace{\int_{x_n=-\infty}^{\infty}\delta\left(x_n\right)\mathrm{d}x_n}_{=1}[\![\mathbf{u}]\!] = \int_{x_n=-\infty}^{\infty}\boldsymbol{\upsilon}\left(\boldsymbol{x}\right)\delta\left(x_n\right)\mathrm{d}x_n\\ &\approx \int_{x_n=-\infty}^{\infty}\boldsymbol{\upsilon}\left(\boldsymbol{x}\right)\delta_c\left(x_n\right)\mathrm{d}x_n\end{aligned} \tag{25}$$

in which $\boldsymbol{\upsilon}(\boldsymbol{x})$ is an auxiliary field employed to approximate the displacement jump in a smeared sense [15]. $\delta_c\left(x_n\right)$ is the approximated form of the Dirac-delta function $\delta\left(x_n\right)$, i.e. Eq. (12).

Applying the divergence theorem to the weak form equation of Eq. (13) leads to the elastic strain $\boldsymbol{\varepsilon}^e$ [11]:

$$\varepsilon_{ij}^e = u_{(i,j)} - \mathrm{sym}\left(\upsilon_i n_j\right)\delta_c \tag{26}$$

In order to arrive at this equation the variational principle has been employed, and $u_{(i,j)} = \frac{1}{2}\left(\frac{\partial u_i}{\partial x_j} + \frac{\partial u_j}{\partial x_i}\right)$ and n_j being the component of the unit vector normal to the interface Γ_c.

Eq. (26) can also be derived in the framework of the extended finite element method (XFEM) [15]. The displacement function in the XFEM is given as

$$\mathbf{u}\left(\mathbf{x}\right) = \mathbf{w}\left(\mathbf{x}\right) + \mathscr{H}\left(\mathbf{x}\right)\boldsymbol{\upsilon}\left(\mathbf{x}\right) \tag{27}$$

with $\mathbf{w}(\mathbf{x})$ being a continuous displacement function, $\boldsymbol{\upsilon}(\mathbf{x})$ being the crack opening function, $\mathscr{H}$ being the Heaviside function, defined as [19]

$$\mathscr{H}\left(\boldsymbol{x}\right) = \frac{1}{2}\begin{cases}1 & \pi\ell/2 \le x_n\\ \sin\left(\frac{x_n}{\ell}\right) & -\pi\ell/2 \le x_n \le \pi\ell/2\\ -1 & \text{otherwise}\end{cases} \tag{28}$$

Due to the small strain assumption, the strain field is then obtained as [24]

$$\varepsilon_{ij} = u_{(i,j)} = \mathrm{w}_{(i,j)} + \mathscr{H}\upsilon_{(i,j)} + \mathrm{sym}\left(\upsilon_i n_j\right)\delta_c \tag{29}$$

which is identical to Eq. (26) under the assumption that $\varepsilon_{ij}^e = \mathrm{w}_{(i,j)} + \mathscr{H}\upsilon_{(i,j)}$.

Multiplying Eq. (27) with the normal vector $\boldsymbol{n}$, defined in Eq. (18), and integrating over the normal direction $x_n \in [-\infty\ \infty]$, we obtain an approximated form of the crack opening in the normal direction for the cohesive fracture model:

$$[\![\mathbf{u}\cdot\boldsymbol{n}]\!] = \boldsymbol{\upsilon}\left(\boldsymbol{x}\right)\cdot\boldsymbol{n} \approx -2\int_{-\infty}^{\infty}\mathbf{u}\left(x_n\right)\cdot\left(\nabla d\left(x_n\right)\mathbf{I}\right)\mathrm{d}x_n \tag{30}$$

where Eq. (15) has been used. The factor '2' stems from the fraction $\frac{1}{2}$ in Eq. (28). Similarly, we can obtain the crack sliding in the shear direction:

$$[\![\mathbf{u}\cdot\boldsymbol{s}]\!] = \boldsymbol{\upsilon}\left(\boldsymbol{x}\right)\cdot\boldsymbol{s} \approx -2\int_{-\infty}^{\infty}\mathbf{u}\left(x_n\right)\cdot\left(\nabla d\left(x_n\right)\mathbf{I}_a\right)\mathrm{d}x_n \tag{31}$$

where Eqs. (15) and (21) have been used. Hence, the displacement jump at the crack can be approximated as:

$$\begin{aligned}&\left[[\![\mathbf{u}\cdot\boldsymbol{n}]\!] \quad [\![\mathbf{u}\cdot\boldsymbol{s}]\!]\right]\\ &\quad\approx -2\int_{-\infty}^{\infty}\left[\mathbf{u}\left(x_n\right)\cdot\left(\nabla d\left(x_n\right)\mathbf{I}\right) \quad \mathbf{u}\left(x_n\right)\cdot\left(\nabla d\left(x_n\right)\mathbf{I}_a\right)\right]\mathrm{d}x_n\end{aligned} \tag{32}$$

In the examples we will employ Eqs. (24) and (32) to compute the displacement jump at the crack for brittle and cohesive fracture, respectively. For the brittle fracture model, we minimise the total energy, i.e., Eq. (6), with respect to the displacement field $\mathbf{u}$. We then obtain the displacement jump at the crack. The cohesive phase-field model includes the displacement $\mathbf{u}$ and the crack opening $[\![\mathbf{u}]\!]$ as

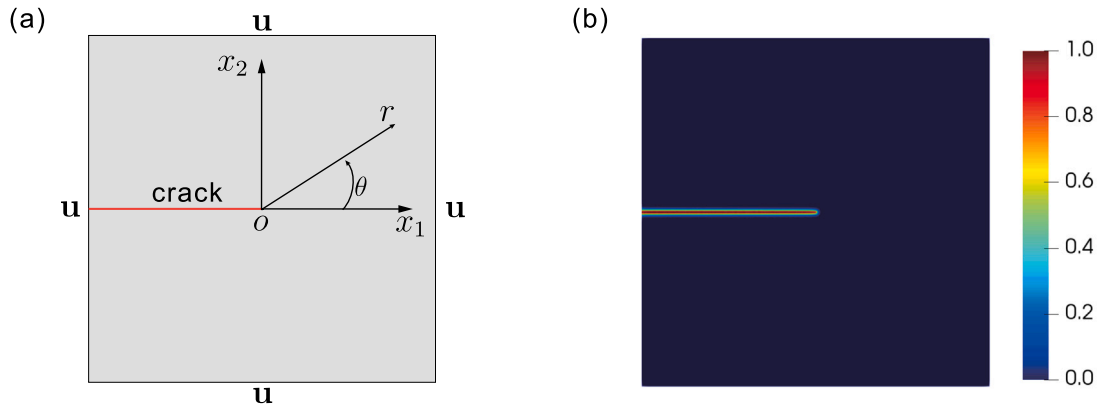

Fig. 2. (a) geometry and boundary conditions for an edge-cracked square plate; (b) smeared representation of the crack. In (a), the initial crack is introduced as the red line.

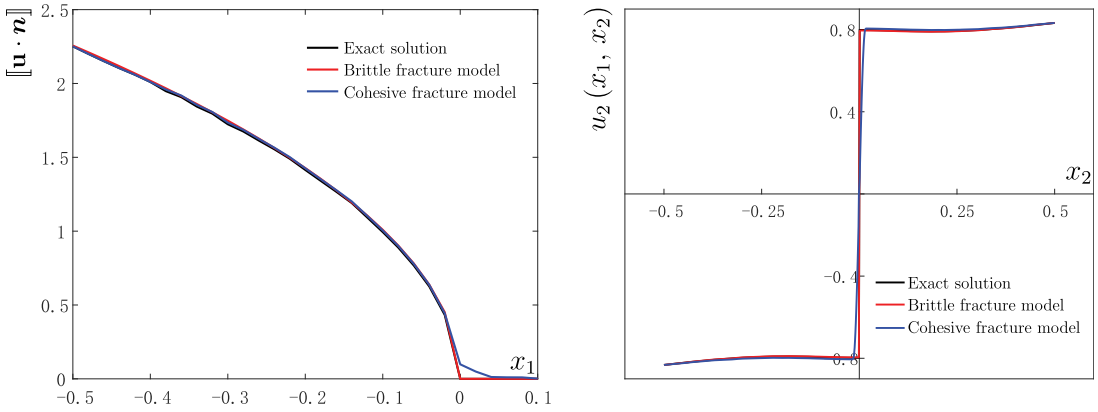

Fig. 3. Crack opening in the normal direction $[\![\mathbf{u}\cdot\boldsymbol{n}]\!]$ (left) and displacement $u_2(x_1, x_2)$ at $x_1 = -0.25$ (right) for Mode-I loading.

variables. Verhoosel and de Borst [11] have proposed a cohesive phase-field model, which uses an auxiliary field $\boldsymbol{v}$ to model $[\![\mathbf{u}]\!]$, required as input in a cohesive-zone model, see also [15]. Herein, we will obtain the displacement $\mathbf{u}$ for the cohesive fracture model, and then use Eq. (32) to compute the displacement jump at the crack.

4. Validation of the crack opening computation

To validate the proposed formulations for the crack opening computation, we consider a square plate (dimension 1×1) with an edge crack, shown in Fig. 2(a). The length of the initial crack is $a = 0.5$. With a suitable re-scaling of the loading the material properties can be chosen as: Young's modulus $E = 1.0$ and Poisson's ratio $\nu = 0.3$. Plane-stress conditions are assumed. Fig. 2(a) shows the geometry and boundary conditions. In the analysis, we consider the Mode-I and Mode-II loading cases separately. The analytical solution of the displacement can be found in [24]. We will solve the problem by the phase field modelling. We consider the problem in a brittle fracture as well as in a cohesive fracture setting. Fig. 2(b) shows the regularised crack, i.e., coloured area, by the phase field model in Section 2.1. The regularisation length is set as $\ell = 0.01$. Next, we will present the results for the Mode-I and Mode-II loading cases, respectively.

4.1. Mode-I loading

The displacement on the boundary of Fig. 2(a) corresponds to Mode-I loading (parameterised by the stress intensity factor $\mathrm{K_I} = 1$ around the initial crack tip). The analytical expressions of displacement field read:

$$\begin{aligned} u_1 &= \frac{\mathrm{K_I}}{2\mu}\sqrt{\frac{r}{2\pi}}\cos\frac{\theta}{2}\left(\kappa - \cos\theta\right) \\ u_2 &= \frac{\mathrm{K_I}}{2\mu}\sqrt{\frac{r}{2\pi}}\sin\frac{\theta}{2}\left(\kappa - \cos\theta\right) \end{aligned} \tag{33}$$

where $\mu = E/2(1+\nu)$, $\kappa = 3-4\nu$ for plane strain and $\kappa = (3-\nu)/(1+\nu)$ for plane stress, and (r, θ) are polar coordinates with the origin positioned at the crack tip.

The closed-form solution for the crack opening displacement is given by:

$$[\![\mathbf{u}]\!](\boldsymbol{x}_c) = \left\{ [\![\mathbf{u}\cdot\boldsymbol{n}]\!] \quad [\![\mathbf{u}\cdot\boldsymbol{s}]\!] \right\} = \left[\frac{\mathrm{K_I}}{\mu}\sqrt{\frac{r}{2\pi}}\left(\kappa + 1\right) \qquad 0 \right] \tag{34}$$

with $\boldsymbol{x}_c$ on the crack. For Mode-I loading we only have the crack opening in the normal direction, as given in Eq. (34).

Fig. 3 shows the comparison between the phase-field solutions and the analytical solutions. The results of the brittle and cohesive fracture models agree well with analytical solutions. For the brittle fracture model, the displacement $u_2(x_1, x_2)$ is discontinuous along the crack, as illustrated in Figs. 3 (right) and 4(a)(left). This discontinuous displacement field stems from the brittle phase field model [1]. For the cohesive fracture model, the displacement $u_2(x_1, x_2)$ shows some differences and is continuous in the range of the regularised crack (coloured area in Fig. 2(b)), due to the continuous Dirac-delta function definition in Eq. (12). The continuous displacement field $u_2(x_1, x_2)$ can also be observed in Fig. 4(a)(right). The plot of $\mathbf{u}\cdot\nabla d$ is shown in Fig. 4(b).

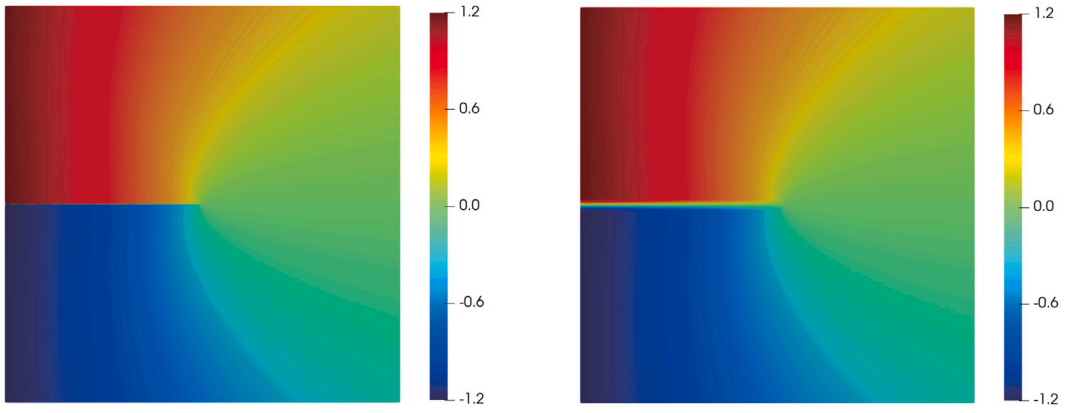

(a) contour plot of displacement u_2

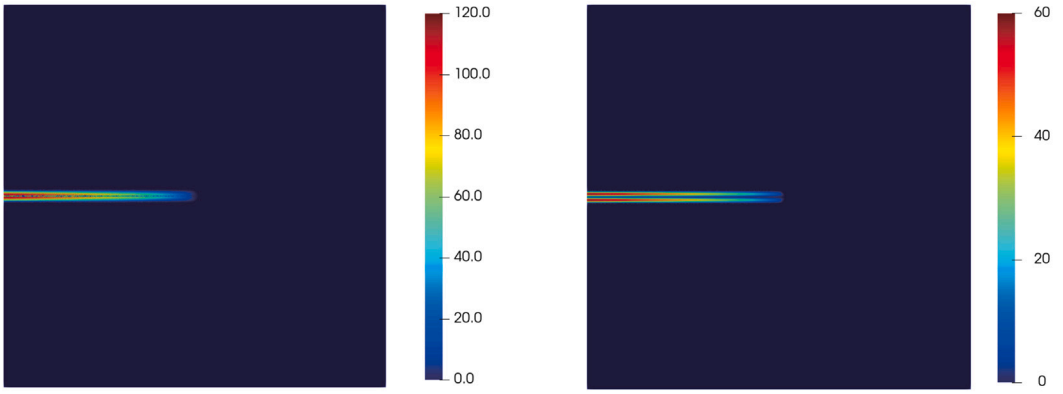

(b) contour plot of $\mathbf{u} \cdot \nabla d$

Fig. 4. Contour plot of displacement u_2 and $\mathbf{u} \cdot \nabla d$ for Mode-I loading. The figures in the left column represent the solution of the brittle fracture model, while the figures in the right column represent the solution of the cohesive fracture model.

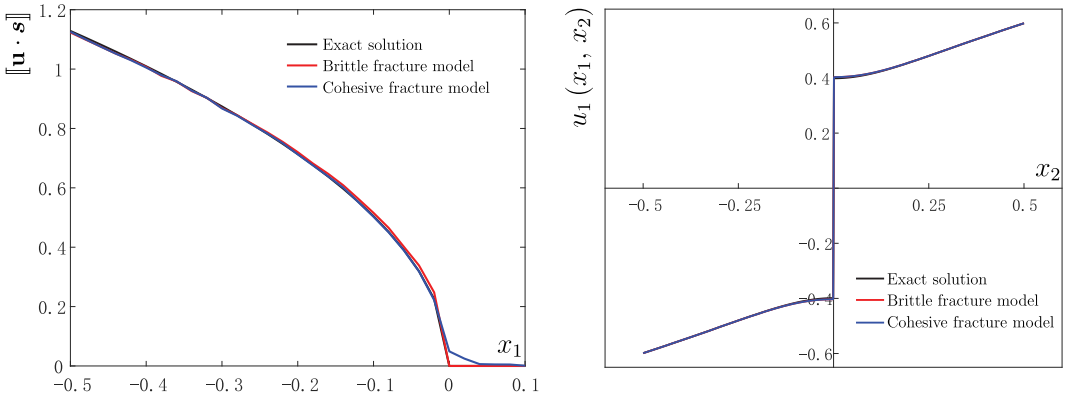

Fig. 5. Crack opening in the normal direction $[\![\mathbf{u} \cdot \boldsymbol{s}]\!]$ (left) and displacement $u_1(x_1\, x_2)$ at $x_1 = -0.25$ (right) for Mode-II loading.

Obviously, the profile of the brittle fracture model differs from that of the cohesive model, due to the difference of the displacement field in Fig. 4(a).

4.2. Mode-II loading

For this loading case, the displacement field is given by

$$\begin{aligned} u_1 &= \frac{\mathrm{K_{II}}}{2\mu}\sqrt{\frac{r}{2\pi}}\sin\frac{\theta}{2}\left(2+\kappa+\cos\theta\right) \\ u_2 &= \frac{\mathrm{K_{II}}}{2\mu}\sqrt{\frac{r}{2\pi}}\cos\frac{\theta}{2}\left(2-\kappa-\cos\theta\right) \end{aligned} \tag{35}$$

with $\mathrm{K_{II}}$ being the stress intensity factor around the initial crack tip, $\mathrm{K_{II}} = 0.5$ in the current study. The closed-form solution for the crack opening displacement is given by:

$$[\![\mathbf{u}]\!](\boldsymbol{x}_c) = \left\{[\![\mathbf{u}\cdot\boldsymbol{n}]\!] \quad [\![\mathbf{u}\cdot\boldsymbol{s}]\!]\right\} = \left[0 \qquad \frac{\mathrm{K_{II}}}{\mu}\sqrt{\frac{r}{2\pi}}\left(\kappa+1\right)\right] \tag{36}$$

as we only have the crack sliding in the shear direction for Mode-II loading.

Fig. 5 shows the results of the crack opening in the shear direction $[\![\mathbf{u}\cdot\boldsymbol{s}]\!]$ and the displacement $u_1(x_1\, x_2)$. As expected, the phase field solutions match well with analytical solutions. Similar to the Mode-I loading case, the displacement of the cohesive fracture model is continuous across the crack, while it is discontinuous in the case of the brittle fracture model, as illustrated in Fig. 6(a). Consequently the profiles of $\mathbf{u}\cdot(\nabla d\,\mathbf{I}_a)$ are different in both models, see Fig. 6(b).

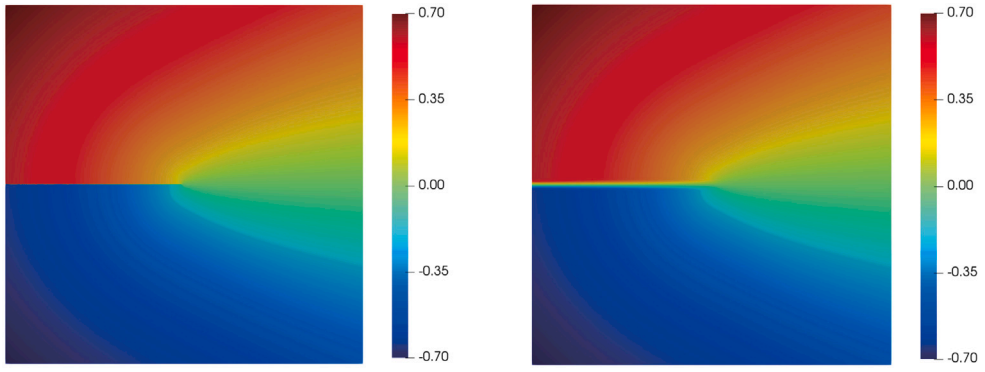

(a) contour plot of displacement u_1

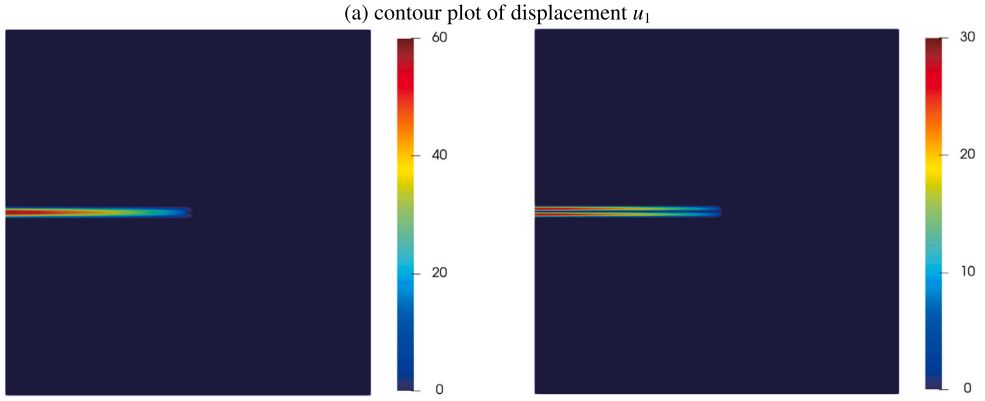

(b) contour plot of $\mathbf{u} \cdot (\nabla d\, \mathbf{I}_a)$

Fig. 6. Contour plot of displacement u_1 and $\mathbf{u} \cdot (\nabla d\, \mathbf{I}_a)$ for Mode-II loading. The figures in the left column represent the solution of the brittle fracture model, while the figures in the right column represent the solution of the cohesive fracture method.

In sum, the brittle and cohesive fracture model will give us different solutions of the displacement. The displacement of the brittle fracture model shows a jump along the crack, while that of the cohesive interface model is continuous, as expected. But both models lead to an identical crack opening displacement, thus validating the proposed formulations.

5. Numerical examples

We now demonstrate the performance of the methodology in a multi-dimensional setting through two representative examples. First, we will consider a curved traction-free crack under uniaxial tension. Both the brittle and cohesive fracture models are employed to obtain the crack opening. Then, a fibre-epoxy debonding test is considered to explore cohesive interface debonding under mixed-mode loading conditions. To well represent the crack in a smeared sense, the regularisation length is always chosen as $l \geq 4h$ (h: element size around the crack) [2].

5.1. Curved crack propagation under uniaxial tension

Mixed-mode crack opening for a curved crack under uniaxial loadings is considered. Fig. 7(a) presents the geometry and boundary conditions. A plane stress state is assumed. With a suitable re-scaling of the loading the material properties can be chosen as: Young's modulus $E = 1.0$ and Poisson's ratio $\nu = 0.3$. An arc crack, starting at (5, 0) and ending at $(5\cos\theta,\ 5\sin\theta)$, is prescribed in the left bottom of the plate. The arc angle is $\theta = 45°$ and the radius of the arc is $R = 5$. The smeared representation of the crack is shown in Fig. 7(b), i.e. the coloured area. To clearly illustrate the smeared crack Γ_ξ, we only present a part of the plate in the figure. The regularisation length is chosen as $\ell = 0.1$. A discrete interface model is used to provide the reference solution [23].

We consider the problem in the setting of brittle fracture and cohesive fracture models, respectively. Fig. 8 presents the profile of the displacement u_1. The results of the phase-field model compare well with those of the discrete interface model. In the figure, the displacement is discontinuous along the crack Γ_c in the brittle fracture model, while it is continuous in the cohesive fracture model, due to the continuous Dirac-delta function definition in Eq. (12). This is also evident in Figs. 9(b) and 10(b). The comparison of the crack opening displacement is shown in Fig. 9(a). Both the normal crack opening $[\![\mathbf{u} \cdot \boldsymbol{n}]\!]$ and the crack sliding $[\![\mathbf{u} \cdot \boldsymbol{s}]\!]$ of the phase-field model, i.e. the brittle and the cohesive fracture model, well match with those of the discrete interface model. This again validates the proposed formulations of the crack opening displacement. Fig. 10 presents the profile of $\mathbf{u} \cdot \nabla d$. Due to the distinct displacement field along the crack Γ_c, the contour plot of $\mathbf{u} \cdot \nabla d$ behaves differently, i.e., discontinuous in the brittle model while continuous in the cohesive model.

5.2. Fibre-epoxy debonding test

We next consider a problem of fibre-epoxy debonding [22]. A cohesive interface is prescribed along the fibre-epoxy boundary. The specimen geometry is shown in Fig. 11(a). Due to symmetry only one quarter of the specimen has been considered with symmetry enforcing boundary conditions. The plate is in a plane-strain condition. The material properties are given as: for the fibre Young's modulus $E = 225$ GPa and Poisson's ratio $\nu = 0.2$, and for the epoxy Young's modulus $E = 4.3$ GPa and a Poisson's ratio $\nu = 0.34$. The Xu–Needleman cohesive zone law is used to describe the fibre-epoxy interface behaviour [22], with $t_u = 50$ MPa and $\mathcal{G}_c = 4 \times 10^{-3}$ N/mm. The cohesive phase field model of Verhoosel and de Borst [11] is used to solve the displacement $\mathbf{u}$. The regularised version of the interface Γ_c is presented in Fig. 11(b), i.e., coloured area. The regularisation length is set as $\ell = 0.05$ μm.

The response curve of the problem has been presented and validated in [15], not shown here for brevity. The profile of computed $\mathbf{u} \cdot \nabla d$ along the interface Γ_c is shown in Fig. 12(a). In the figure, $\mathbf{u} \cdot \nabla d$ is continuous

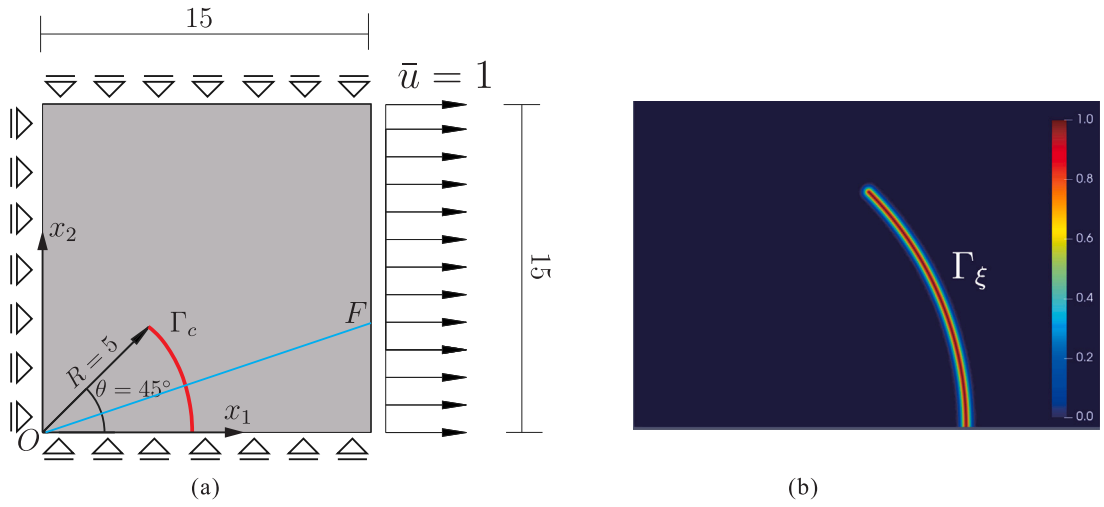

Fig. 7. (a) geometry and boundary conditions for a curved crack problem; (b) smeared representation of the crack. In figure (a), the initial crack Γ_c is introduced as the red line. To clearly show the smeared crack Γ_ξ, Figure (b) only presents the left bottom part of the plate.

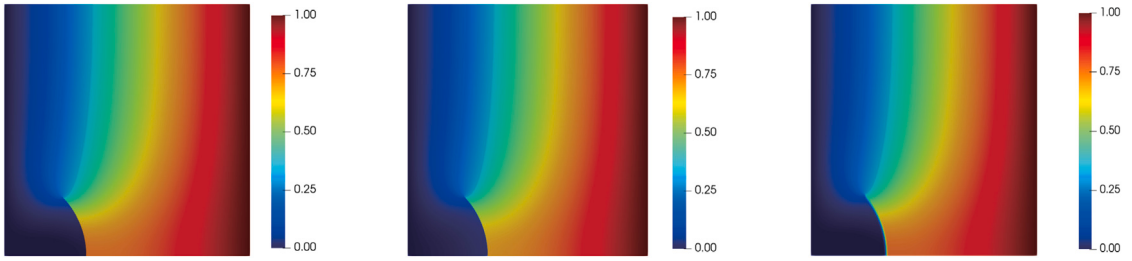

Fig. 8. Distribution of the displacement u_1. Figure (a) is the reference solution. Figures (b) and (c) are the solutions of the phase-field modelling.

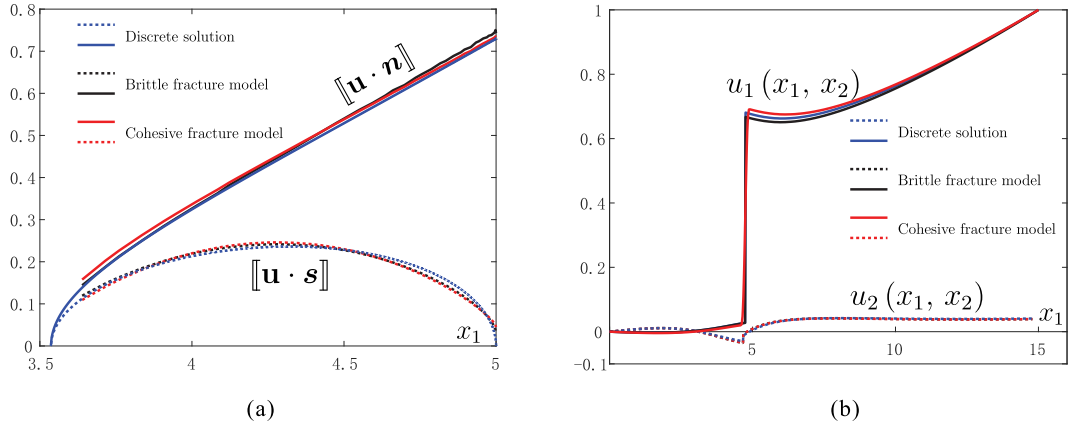

Fig. 9. (a) crack opening in the normal direction $[\![\mathbf{u}\cdot\boldsymbol{n}]\!]$ and in the shear direction $[\![\mathbf{u}\cdot\boldsymbol{s}]\!]$; (b) displacement $u_1(x_1, x_2)$ and $u_2(x_1, x_2)$ along the blue line OF in Fig. 7(a). Point F is with the coordinate $(x_1, x_2) = (15, 5)$.

and confined to a local area around the crack. In Fig. 12(b), we compare the crack opening displacement of Eq. (32) with that of the discrete interface model [22]. Clearly, the results agree well with the discrete interface solution. The displacements and the stresses in the fibre and epoxy are shown in Fig. 13. The results of the 'smeared' model compare well with those of the discrete interface model, though there are some oscillations in the plot around the smeared interface Γ_ξ.

6. Concluding remarks

The phase-field model has found extensive use in the analysis of fracture thanks to its straightforward description of cracks and ease of implementation. The model regularises the crack in a smeared sense and has been applied to brittle and cohesive fracture analysis. In the phase-field approach, the evaluation of the crack opening displacement is still an open issue, especially regarding crack sliding, given the unknown location of the crack opening. However, the displacement jump at the crack is essential in cohesive fracture, and also crucial in certain applications within the brittle fracture model, e.g. in hydraulic fracturing. This study presents formulations for the displacement jump at the crack, and verifies the proposed forms for brittle and for cohesive fracture. To the best of our knowledge, this is the first comprehensive

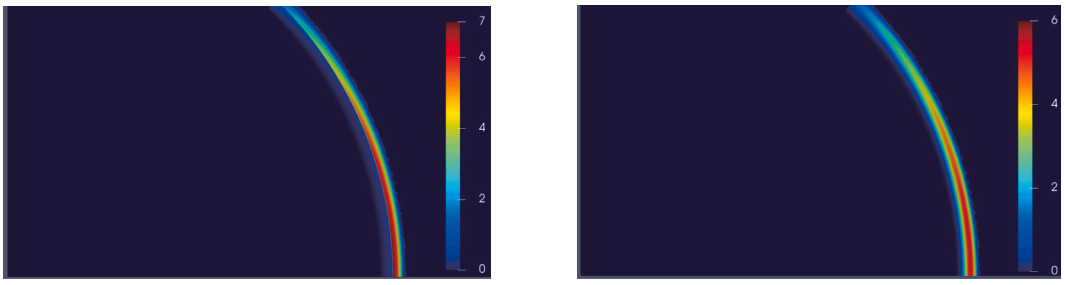

(a) brittle fracture model (b) cohesive fracture model

Fig. 10. Contour plot of $\mathbf{u}\cdot\nabla d$.

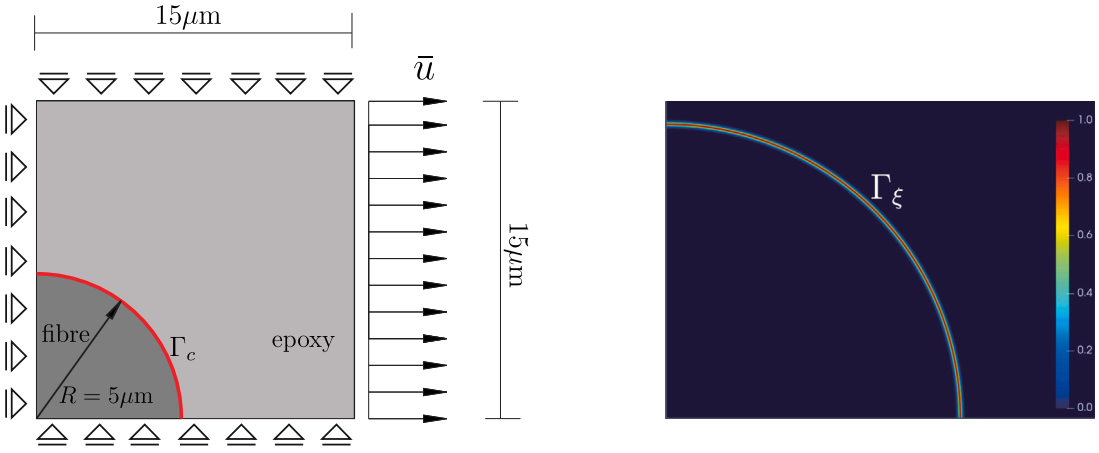

(a) (b)

Fig. 11. (a) geometry and boundary conditions for one quarter of the fibre [22]; (b) smeared representation of the crack. In figure (a), the initial crack Γ_c is introduced as the red line. To clearly show the smeared crack Γ_ξ, Figure (b) only presents the left bottom part of the plate.

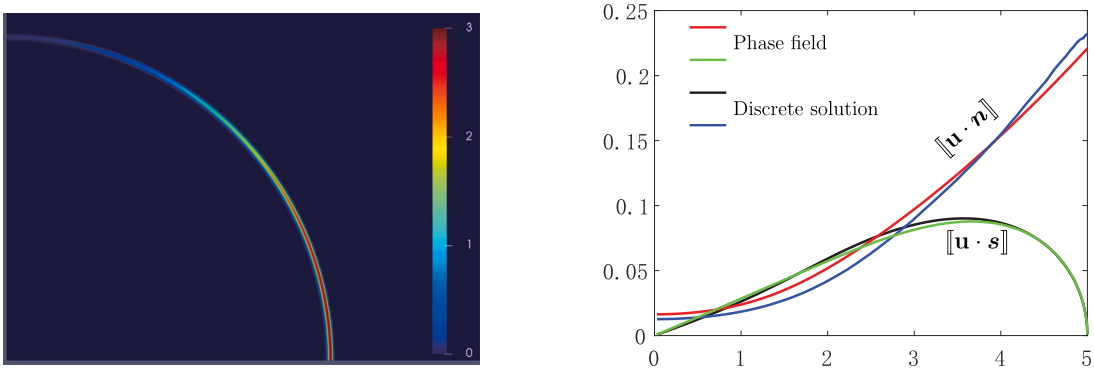

(a) (b)

Fig. 12. (a) contour plot of $\mathbf{u}\cdot\nabla d$ at the loading step $\bar{u}=0.25$ μm; (b) crack opening in the normal direction $[\![\mathbf{u}\cdot\boldsymbol{n}]\!]$ (μm) and in the shear direction $[\![\mathbf{u}\cdot\boldsymbol{s}]\!]$ (μm) along the interface Γ_c at the loading step $\bar{u}=0.25$ μm.

effort to establish a complete formulation of the displacement jump at the crack within the framework of phase-field modelling.

The normal crack opening $[\![\mathbf{u}\cdot\boldsymbol{n}]\!]$ is approximated as the product of a coefficient k and a line integral of $\mathbf{u}\cdot\left(\nabla d\mathbf{I}\right)$ in the direction normal to the crack. The coefficient k is assigned a value $k=1$ for the brittle fracture model, whereas it takes on a value of $k=2$ for the cohesive model. Chukwudozie et al. [6] and Chen et al. [19] have derived an identical form of $[\![\mathbf{u}\cdot\boldsymbol{n}]\!]$ and verified it through benchmarks. For the crack sliding $[\![\mathbf{u}\cdot\boldsymbol{s}]\!]$ the integral term in $[\![\mathbf{u}\cdot\boldsymbol{n}]\!]$ has been replaced by $\mathbf{u}\cdot\left(\nabla d\mathbf{I}_a\right)$, given that the shear crack direction $\boldsymbol{s}$ is orthogonal to the normal crack direction $\boldsymbol{n}$. We have validated the proposed forms of the crack opening displacement analytically, and also numerically in two curved crack problems.

CRediT authorship contribution statement

Lin Chen: Writing – original draft, Software, Formal analysis, Conceptualization. **Bin Li:** Formal analysis, Conceptualization. **René de Borst:** Writing – review & editing.

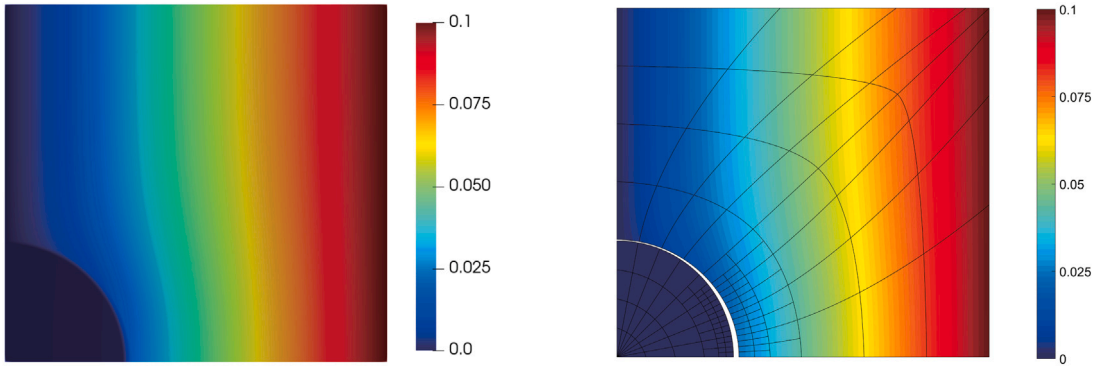

(a) u_1 contour plot

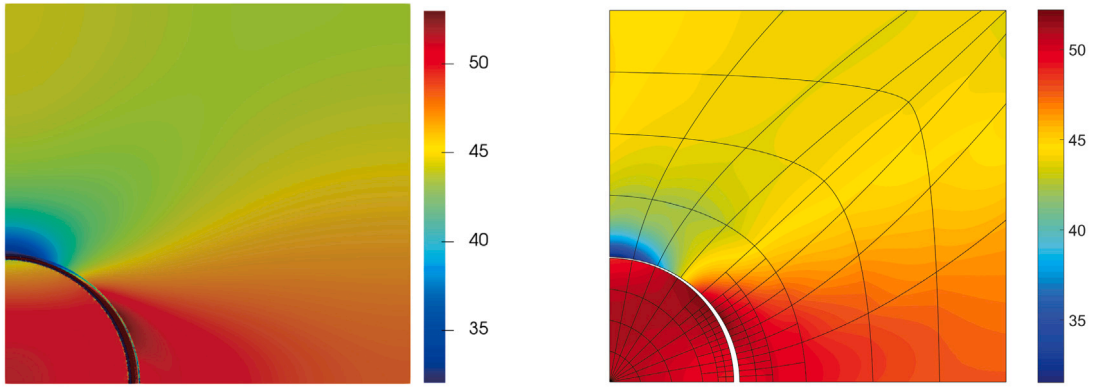

(b) σ_1 contour plot

Fig. 13. Distribution of the displacement u_1 and the stress σ_1 under the loading $\bar{u} = 0.1$ μm. The displacements have been amplified by a factor 10. The left column denotes the solution of phase field method, while the right column represents the solution of the discrete interface model.

Declaration of competing interest

The authors declare that they have no known competing financial interests or personal relationships that could have appeared to influence the work reported in this paper.

Data availability

No data was used for the research described in the article.

References

[1] B. Bourdin, G.A. Francfort, J.J. Marigo, Numerical experiments in revisited brittle fracture, J. Mech. Phys. Solids 48 (2000) 797–826.
[2] B. Bourdin, G.A. Francfort, J.J. Marigo, The variational approach to fracture, J. Elasticity 91 (2008) 5–148.
[3] Y. Heider, A review on phase-field modeling of hydraulic fracturing, Eng. Fract. Mech. 253 (2021) 107881.
[4] C. Miehe, M. Hofacker, L.-M. Schänzel, F. Aldakheel, Phase field modeling of fracture in multi-physics problems. Part II. Coupled brittle-to-ductile failure criteria and crack propagation in thermo-elastic–plastic solids, Comput. Methods Appl. Mech. Engrg. 294 (2015) 486–522.
[5] R. Alessi, S. Vidoli, L. De Lorenzis, A phenomenological approach to fatigue with a variational phase-field model: The one-dimensional case, Eng. Fract. Mech. 190 (2018) 53–73.
[6] C. Chukwudozie, B. Bourdin, K. Yoshioka, A variational phase-field model for hydraulic fracturing in porous media, Comput. Methods Appl. Mech. Engrg. 347 (2019) 957–982.
[7] T. Li, J.-J. Marigo, D. Guilbaud, S. Potapov, Gradient damage modeling of brittle fracture in an explicit dynamics context, Internat. J. Numer. Methods Engrg. 108 (2016) 1381–1405.
[8] M.J. Borden, C.V. Verhoosel, M.A. Scott, T.J.R. Hughes, C.M. Landis, A phase-field description of dynamic brittle fracture, Comput. Methods Appl. Mech. Engrg. 217–220 (2012) 77–95.
[9] K. Yoshioka, D. Naumov, O. Kolditz, On crack opening computation in variational phase-field models for fracture, Comput. Methods Appl. Mech. Engrg. 369 (2020) 113210.
[10] B. Werner, V. Myrseth, A. Saasen, Viscoelastic properties of drilling fluids and their influence on cuttings transport, J. Pet. Sci. Eng. 156 (2017) 845–851.
[11] C.V. Verhoosel, R. de Borst, A phase-field model for cohesive fracture, Internat. J. Numer. Methods Engrg. 96 (2013) 43–62.
[12] J. Vignollet, S. May, R. de Borst, C.V. Verhoosel, Phase-field models for brittle and cohesive fracture, Meccanica 49 (2014) 2587–2601.
[13] S. May, J. Vignollet, R. de Borst, A numerical assessment of phase-field models for brittle and cohesive fracture: Γ-convergence and stress oscillations, Eur. J. Mech. A Solids 52 (2015) 72–84.
[14] Y. Ghaffari Motlagh, R. de Borst, Considerations on a phase-field model for adhesive fracture, Internat. J. Numer. Methods Engrg. 121 (2020) 2946–2963.
[15] L. Chen, R. de Borst, Phase-field regularised cohesive zone model for interface modelling, Theor. Appl. Fract. Mech. 122 (2022) 103630.
[16] T.-T. Nguyen, J. Yvonnet, Q.-Z. Zhu, M. Bornert, C. Chateau, A phase-field method for computational modeling of interfacial damage interacting with crack propagation in realistic microstructures obtained by microtomography, Comput. Methods Appl. Mech. Engrg. 312 (2016) 567–595.
[17] R. de Borst, L. Chen, Phase-field modelling of cohesive interface failure, Internat. J. Numer. Methods Engrg. (2023) e7412.
[18] S. Lee, M.F. Wheeler, T. Wick, Iterative coupling of flow, geomechanics and adaptive phase-field fracture including level-set crack width approaches, J. Comput. Appl. Math. 314 (2017) 40–60.
[19] L. Chen, Z. Wang, B. Li, R. de Borst, Computation of the crack opening displacement in the phase-field model, Int. J. Solids Struct. 283 (2023) 112496.
[20] D.S. Dugdale, Yielding of steel sheets containing slits, J. Mech. Phys. Solids 8 (1960) 100–104.
[21] G.I. Barenblatt, The mathematical theory of equilibrium cracks in brittle fracture, Adv. Appl. Mech. 7 (1962) 55–129.
[22] L. Chen, F.J. Lingen, R. de Borst, Adaptive hierarchical refinement of NURBS in cohesive fracture analysis, Internat. J. Numer. Methods Engrg. 112 (2017) 2151–2173.
[23] L. Chen, R. de Borst, Cohesive fracture analysis using Powell-Sabin B-splines, Int. J. Numer. Anal. Methods Geomech. 43 (2019) 625–640.
[24] L. Chen, H. Bahai, G. Alfano, Extended Powell–Sabin finite element scheme for linear elastic fracture mechanics, Eng. Fract. Mech. 274 (2022) 108719.